Icarus **158**, 379–388 (2002)
doi:10.1006/icar.2002.6869

Radar Observations of Asteroid 3908 Nyx

Lance A. M. Benner and Steven J. Ostro

Jet Propulsion Laboratory, California Institute of Technology, Pasadena, California 91109-8099
E-mail: lance@reason.jpl.nasa.gov

R. Scott Hudson

School of Electrical Engineering and Computer Science, Washington State University, Pullman, Washington 99164-2752

Keith D. Rosema,[1] Raymond F. Jurgens, and Donald K. Yeomans

Jet Propulsion Laboratory, California Institute of Technology, Pasadena, California 91109-8099

Donald B. Campbell

National Astronomy and Ionosphere Center, Space Sciences Building, Cornell University, Ithaca, New York 14853

and

John F. Chandler and Irwin I. Shapiro

Harvard–Smithsonian Center for Astrophysics, 60 Garden Street, Cambridge, Massachusets 02138

Received August 30, 2001; revised February 21, 2002

We report Doppler-only (cw) radar observations of basaltic near-Earth asteroid 3908 Nyx obtained at Arecibo and Goldstone in September and October of 1988. The circular polarization ratio of 0.75 ± 0.03 exceeds ∼90% of those reported among radar-detected near- Earth asteroids and it implies an extremely rough near-surface at centimeter-to-decimeter spatial scales. Echo power spectra over narrow longitudinal intervals show a central dip indicative of at least one significant concavity. Inversion of cw spectra yields two statistically indistinguishable shape models that have similar shapes and dimensions but pole directions that differ by ∼100°. We adopt one as our working model and explore its implications. It has an effective diameter of 1.0 ± 0.15 km and radar and visual geometric albedos of 0.15 ± 0.075 and $0.16^{+0.08}_{-0.05}$. The visual albedo supports the interpretation by D. P. Cruikshank *et al.* (1991, *Icarus* 89, 1–13) that Nyx has a thermal inertia consistent with that of bare rock. The model is irregular, modestly asymmetric, and topographically rugged.

Key Words: **asteroids; radar.**

INTRODUCTION

3908 Nyx (1980 PA), one of only a few known basaltic (i.e., V-class) near-Earth asteroids (NEAs) (Cruikshank *et al.* 1991), was discovered on August 6, 1980, by H.-E. Schuster at the European Southern Observatory in La Silla (Marsden 1980). It was the subject of an extensive observational campaign at visible, infrared, and radar wavelengths during its approach within 0.062 AU of Earth in October 1988. Lightcurves obtained in 1988 (Drummond and Wisniewski 1990) and in 1996 by Pravec and co-workers (in preparation) indicate direct rotation with a 4.426-h period and yield two pole direction solutions that provide comparably good fits to the data. Cruikshank *et al.* (1991) obtained infrared radiometric observations of Nyx and applied three thermal models to estimate the visual geometric albedo and effective diameter: the standard, dusty, and rocky models. They favor the conservative rocky model, which gives a visual geometric albedo of about 0.2 and a diameter of about 1 km. The other thermal models imply smaller diameters and geometric albedos, ∼0.5 to 0.6, that are higher than almost all other asteroid albedos. Table I summarizes Nyx's optically derived physical properties.

Here we report results of Doppler-only (i.e., continuous wave or CW) observations at Arecibo and Goldstone in 1988 (Table II). Echoes obtained using the highest range resolution setups available in 1988 yielded images that placed only 2–3 range pixels on the target, so we limit our analysis to the much better resolved CW echoes. Delay-Doppler astrometry for Nyx was reported by Ostro *et al.* (1991) and is also available on the Internet at the JPL Solar System Dynamics Web site at http://ssd.jpl.

[1] Current address: Blue Origin, LLC. 13 South Nevada Street, Seattle, WA 98134.

0019-1035/02 $35.00

TABLE I
Optically Estimated Physical Properties

Property	Value	References
Absolute magnitude H (mag)	17.54 ± 0.04	2
	17.56 ± 0.01	1
	17.55 ± 0.03	3
Taxonomic class	V	1
Rotation period P (h)	4.426 ± 0.001	2, 3
Rotation sense	Direct	2, 3
Lightcurve amplitude Δm (mag)	$0.25 - 0.45$	2, 3
Ecliptic longitude λ (°)	312 ± 10	2 (model 1)
	177 ± 11	2 (model 2)
	330 ± 25	3 (model 1)
	168 ± 20	3 (model 2)
Ecliptic latitude β (°)	$+61 \pm 10$	2 (model 1)
	$+23 \pm 11$	2 (model 2)
	$+52 \pm 10$	3 (model 1)
	$+25 \pm 10$	3 (model 2)
Standard thermal model		
Visual albedo p_v	0.57 ± 0.08	1
Effective diameter D_{eff} (km)	0.62 ± 0.04	1
"Dusty" thermal model		
p_v	0.46 ± 0.07	1
D_{eff} (km)	0.68 ± 0.02	1
"Rocky" thermal model		
p_v	0.23 ± 0.04	1
D_{eff} (km)	0.98 ± 0.04	1
Major axis ratios		
a/b	1.36 ± 0.03	2 (model 1)
	1.20 ± 0.01	2 (model 2)
	1.21 ± 0.06	3
b/c	1.27 ± 0.03	2 (model 1)
	1.11 ± 0.01	2 (model 2)
	1.11 ± 0.05	3

Note. References: (1) Cruikshank *et al.* (1991); (2) Drummond and Wisniewski (1990); (3) Pravec and co-workers (in preparation).

nasa.gov/radar_data.html. Our observations and modeling of its shape and size reveal that Nyx is an irregularly shaped object close to 1 km in diameter with substantial roughness at decimeter scales.

ANALYSIS OF SPECTRA

Our methods of radar data reduction and analysis follow those described in detail by Ostro *et al.* (1992, 1996). In Doppler-only observations, echoes were received simultaneously in the opposite (OC) and same (SC) senses of circular polarization as the transmission. Uncertainties in the radar cross section are dominated by systematic pointing and calibration errors. We assign standard errors of 50% to the radar cross section. The circular polarization ratio SC/OC is a gauge of near-surface roughness at spatial scales within about an order of magnitude of the radar wavelength. Errors in the measured ratios are small because virtually all systematic errors apply equally to both the OC and SC cross sections. All stated uncertainties are one standard deviation.

Figures 1 and 2 show weighted sums of spectra obtained on each day at Arecibo and Goldstone. Weighted sums of spectra obtained in the sense of circular polarization opposite from that transmitted give signal-to-noise ratios (SNRs) of about 240 for Arecibo and about 70 for Goldstone. Nyx's OC radar cross sections, 0.13 ± 0.065 km^2 at 13 cm and 0.09 ± 0.045 km^2 at 3.5 cm, were reported by Ostro *et al.* (1991).

Our estimates of the circular polarization ratio, SC/OC, are 0.78 ± 0.02 at 13 cm and 0.72 ± 0.04 at 3.5 cm (the uncertainty is

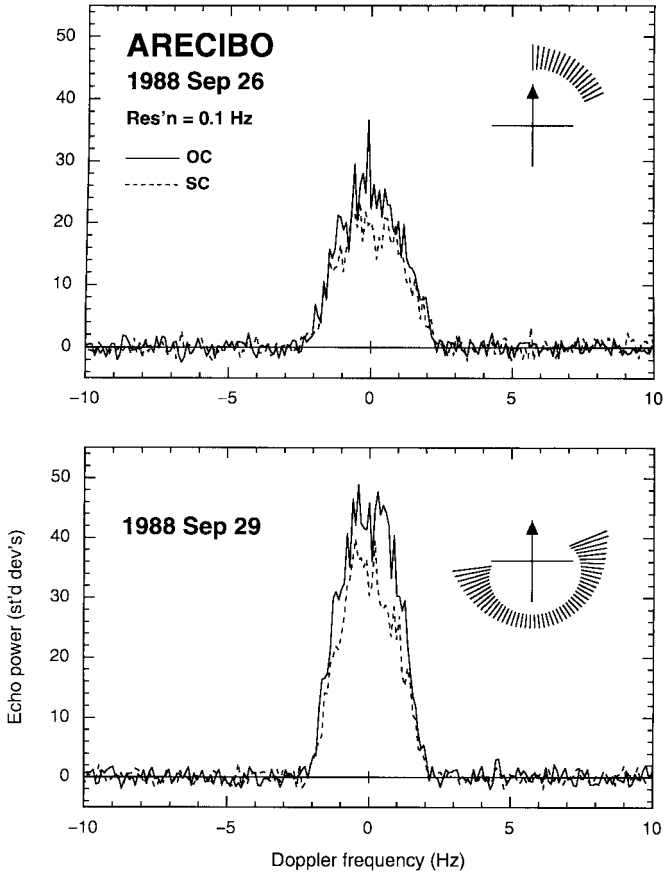

FIG. 1. Arecibo echo power spectra from September 26 and 29 at the raw 0.1-Hz resolution. Echo power is plotted in standard deviations versus Doppler frequency relative to the estimated frequency of echoes from the asteroid's center of mass. Solid and dashed curves denote echo power in the OC and SC polarizations. Rotation phase coverage is indicated with inset crosses and radial line segments based on a synodic rotation period of 4.426 h, where the arrow at 12 o'clock indicates zero phase, rotation phase increases clockwise, and the zero phase epoch is 1988 September 26 02 : 10 : 23 UTC. Radial line segment lengths are proportional to the standard deviation of each spectrum. A vertical bar at zero Hz indicates ±1 standard deviation.

TABLE II
Radar Observations

Date	Setup	RA (°)	DEC (°)	Distance (AU)	P_{tx} (kW)	Runs	UTC receive hhmmss-hhmmss
			Arecibo				
1988 Sep 26	0.1 Hz	343.17	24.87	0.081	440	17	021023-025935
	20 μs					4	033030-034111
	20.5 μs					4	034410-035457
	4 μs					5	040200-041601
1988 Sep 27	6 μs	344.49	26.27	0.079	430	8	015830-022737
	2 μs					25	023050-034757
1988 Sep 28	2 μs	345.93	27.72	0.077	430	30	022240-034721
1988 Sep 29	0.1 Hz	347.50	29.23	0.075	440	49	014917-041430
			Goldstone				
1988 Oct 06	1.95 Hz	4.14	40.76	0.064	360	32	065907-082617
	5 μs					17	091250-095428
1988 Oct 12	0.49 Hz	26.37	48.09	0.062	370	20	033036-041945
	5 μs					14	045753-053015
	5.125 μs					7	053829-055330
1988 Oct 19	1.375 μs	55.66	49.08	0.067	370	100	062146-104600
1988 Oct 24	0.49 Hz	71.18	45.92	0.074	370	45	054338-083100
1988 Oct 25	0.49 Hz	73.67	45.11	0.076	370	107	035935-101045

Note. Setup indicates delay and Doppler resolution. The transmitter frequency was 2380 MHz at Arecibo and 8495 MHz at Goldstone. Right ascension, declination, and distance are given for the midpoints of the observations. P_{tx} is the transmitter power. The number of transmit/receive cycles (runs) is indicated in the seventh column.

due to receiver noise) (Ostro *et al.* 1991). Among radar-detected NEAs that have been reported, SC/OC for Nyx ranks fifth highest (Table III) out of ∼100 radar-detected NEAs and it is considerably larger than the ratios estimated for basaltic main-belt Asteroid 4 Vesta, which average 0.28 ± 0.05 (Mitchell *et al.* 1996). (Preliminary results from recent radar observations of NEAs 1998 WT24 and 4660 Nereus revealed SC/OC comparable to that of Nyx at 13 cm and 3.5 cm.) Nyx and 1981 Midas (Ostro *et al.* 1991), which is also a basaltic NEA (Binzel *et al.* 2001), have similar SC/OC values. The high ratio indicates that Nyx is extremely rough at decimeter spatial scales. The near-surface of Nyx is considerably rougher than that of 433 Eros, which has an average circular polarization ratio at 13 cm of 0.22 ± 0.06 (Ostro *et al.* 1991, Magri *et al.* 2001). There is no evidence for variation of the disc-integrated SC/OC ratio with rotation phase.

Figures 3 and 4 show sums of spectra grouped into 20°–30° rotation phase intervals. A subset of the Arecibo spectra show evidence for modest asymmetry in the shape and several Arecibo spectra are approximately triangular. The Arecibo bandwidths estimated using the two-sigma levels as an edge detection threshold vary by only ∼20%, indicating that Nyx's

TABLE III
Highest NEA Circular Polarization Ratios

Rank	Object		SC/OC	Reference
1	17511	1992 QN	1.10 ± 0.19	Benner *et al.* 1997
		2000 EE104	1.1 ± 0.3	Howell *et al.* 2001
3	2101	Adonis	1.02 ± 0.11	Benner *et al.* 1997
4	3103	Eger	0.92 ± 0.06	Benner *et al.* 1997
5	3908	Nyx	0.75 ± 0.03	This paper
6	1981	Midas	0.65 ± 0.13	Ostro *et al.* 1991
7	1566	Icarus	0.5 ± 0.2	Mahapatra *et al.* 1999
		1998 KY26	0.5 ± 0.1	Ostro *et al.* 1999

Note. SC/OC for Eger, Nyx, and Midas are the averages of 13-cm and 3.5-cm estimates.

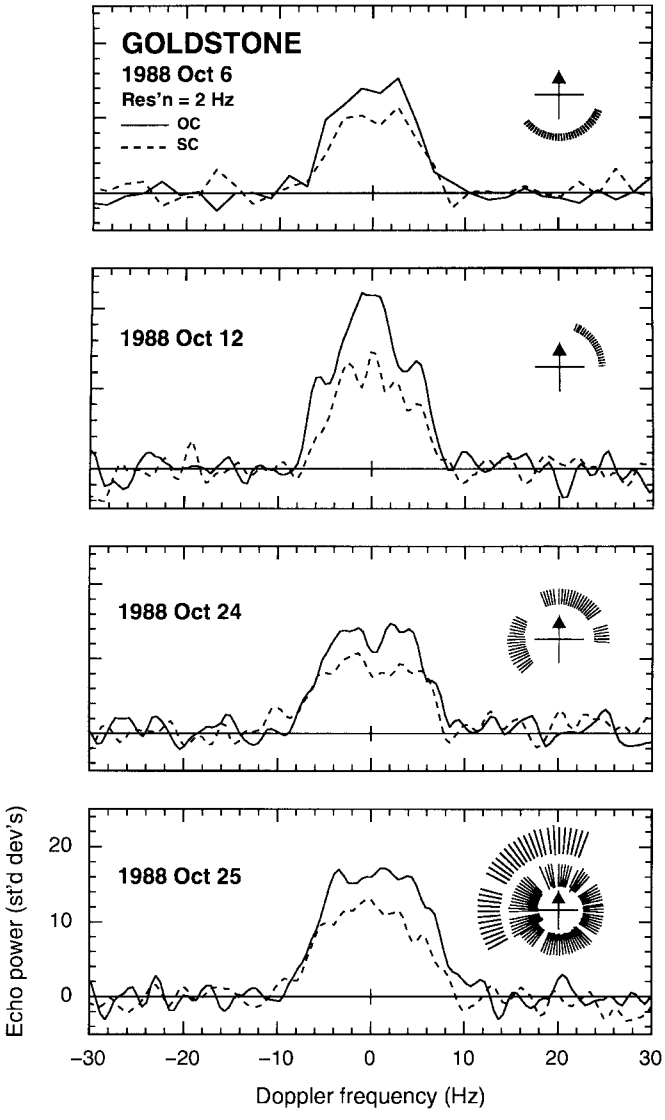

FIG. 2. Goldstone echo power spectra from October 6, 12, 24, and 25 at 2-Hz resolution. Rotation phase coverage is indicated using the same notation and zero phase epoch as in Fig. 1. Concentric rings (beginning with the inner ring) on October 25 indicate successive rotations of the asteroid relative to the start of observations on that day.

pole-on silhouette is not highly elongated. The other 15 near-Earth asteroids for which useful radar-derived shape information is available have elongations ranging from 1.1 to 2.5, with a median of 1.4 and a mean and rms dispersion of 1.6 ± 0.4. Thus, Nyx is among the least elongated NEAs in the radar sample.

Figure 5 shows Arecibo and Goldstone spectra that have prominent central dips, which are probably evidence of one or more concavities. The Arecibo spectrum shows that SC/OC increased at frequencies at the middle of the dip; this is the signature expected for a double reflection and is reminiscent of the signature seen in echoes obtained from contact-binary-shaped object 4769 Castalia (Ostro *et al.* 1990). Prominent central dips have also been observed in echoes from bifurcated asteroids 2063 Bacchus (Benner *et al.* 1999) and 4486 Mithra (Ostro *et al.* 2000).

PHYSICAL MODEL

Given sufficient SNR, orientational coverage of the surface, and estimates of the spin vector, all of which are available for Nyx, Doppler-only spectra can be inverted to reconstruct an object's three-dimensional shape using the techniques described by Hudson (1993) and applied by Hudson and Ostro (1994, 1995) to reconstruct the shapes of 4769 Castalia and 4179 Toutatis. Shape models have been constructed from Doppler-only radar data for NEAs 433 Eros (Mitchell *et al.* 1998) and 1998 KY26 (Ostro *et al.* 1999), and the Eros shape was subsequently verified by the NEAR spacecraft (Veverka *et al.* 1999).

We began with a grid search with 5° resolution over all possible pole directions by fitting an ellipsoid to all the Arecibo and Goldstone data. A difference of 4% is statistically significant at the 1σ level for these data, which contain 1456 independent data points. We obtained four candidate pole directions that give comparably good fits to the data, but we limit the poles we consider to direct pole directions because Drummond and Wisniewski (1990) and Pravec and co-workers (in preparation) conclude that retrograde pole directions give statistically inferior fits to the lightcurves.

The two prograde solutions, with ecliptic longititudes and latitudes $(\lambda, \beta) = (43^\circ \pm 30^\circ, +71^\circ \pm 15^\circ)$ and $(198^\circ \pm 30^\circ, +5^\circ \pm 15^\circ)$, are separated by about 100° and have χ^2 values that differ by only ∼2%, which is statistically insignificant. The solutions differ by a few tens of degrees from those obtained by Drummond and Wisniewski (1990), and Pravec and co-workers (Table I).

At their raw resolution of 0.1 Hz, the Arecibo spectra provide strong echoes but have fractional self noise of about 38% at echo-containing frequencies because there are only seven FFTs (i.e., looks) in each run (transmit–receive cycle). Consequently, as a compromise between reducing self noise (to avoid fitting the noise) and increasing rotational smear, we smoothed the Arecibo spectra to ∼25° rotation phase intervals (i.e., seven runs), which produced spectra with self noise of about 14%. We then smoothed the data in frequency to a resolution of 0.4 Hz, reducing the self noise to ∼7%. We grouped the much weaker Goldstone spectra into ∼30° rotation phase intervals and smoothed them to a frequency resolution of 2 Hz. Smoothing by 25°–30° of rotation phase has a more pronounced effect on the spectra than the smoothing in Doppler frequency. We explored including the Goldstone spectra in the modeling but found that they are too weak to be useful.

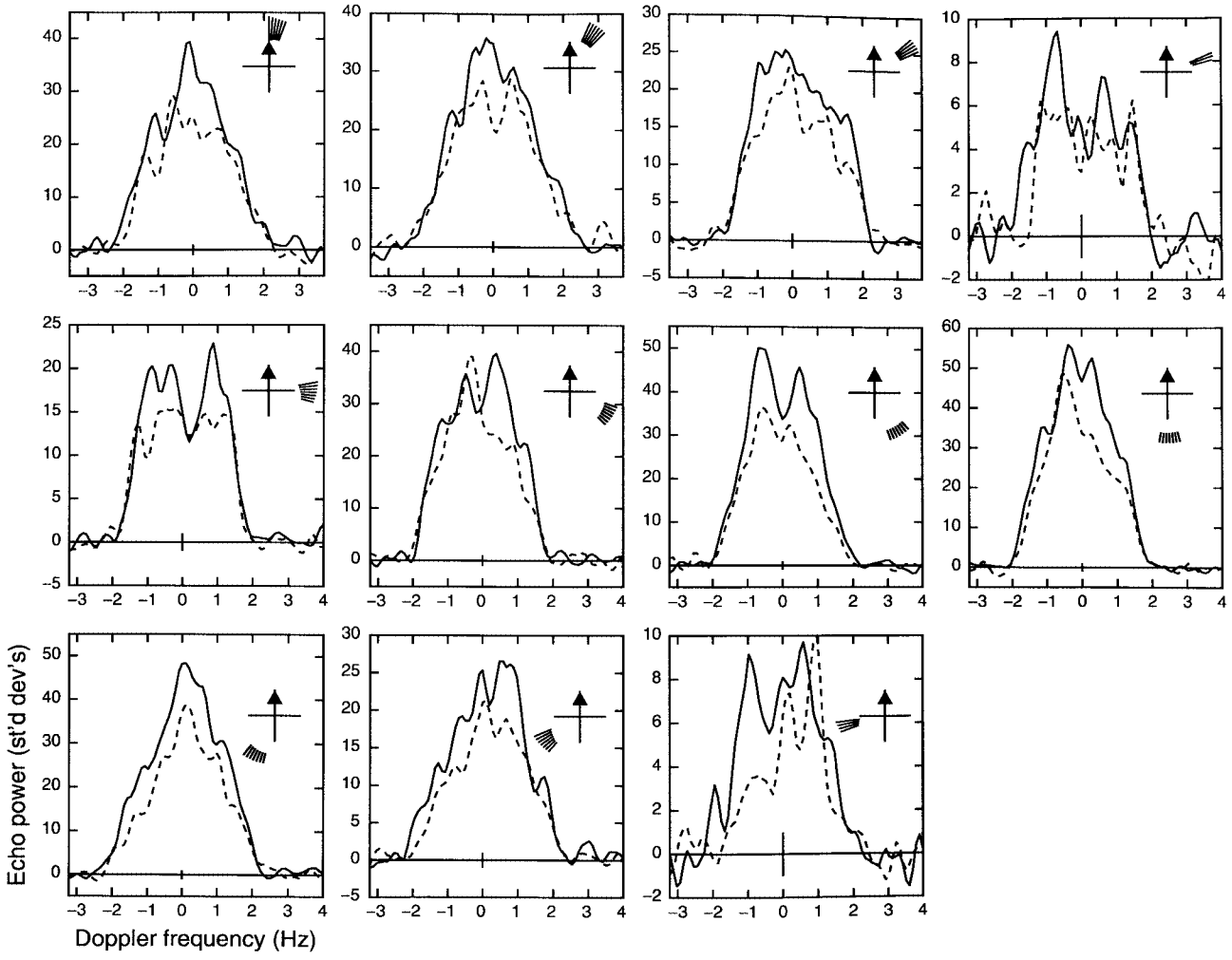

FIG. 3. Evolution of Arecibo echo power spectra on September 26 and 29. Rotation phase (time) increases from left to right and from top to bottom. Each spectrum is a weighted sum spanning an average of about 25° of rotation phase and has been filtered to a frequency resolution of 0.4 Hz. Different vertical scales are used on each panel. Rotational phase coverage is indicated as in Fig. 1.

The models are specified by 256 vertex shape parameters, 11 calibration factors (one for each spectrum), and two factors for the pole direction (following the approach in Mitchell *et al.* 1998), for a total of 269 free parameters. We fit the data with two models, each initialized to one of the candidate pole solutions (which were allowed to float). The two poles yield models with statistically indistinguishable fits and very similar model dimensions and shapes, so we adopted one ($\lambda = 43°, \beta = +71°$) as our working model and explore its implications. The principal difference is the effective diameter, which is about 10% larger for the working model. We constrained the spin state to correspond to a homogeneous body in principal axis rotation. We adopted a radar scattering law in the form $\sigma_0 = \rho \cos^n(\theta)$, where ρ describes the reflectivity of the surface at normal incidence, n indicates the degree of specularity, and θ is the angle of incidence at a point on the surface. Because of Nyx's high circular polarization ratio, we assumed that scattering is Lambertian and fixed $n = 2$. The objective function that we minimized included weighted penalty terms used to suppress nonsmoothness of the model, i.e., sharp edges and concavities (Hudson and Ostro 1994, 1995). The weightings were increased until χ^2 rose significantly, where a 6% increase in χ^2 is significant at the one standard deviation level for these data, which have 418 independent data points.

We varied penalty weights in unison and individually over four orders of magnitude and explored their effects on the fits. The smallest penalty weights give very irregular shapes and better fits but obviously are fitting the noise; conversely, high penalty weights produce worse fits and smoother shapes. As a compromise between these extremes, we adopt conservative roughness and concavity penalty weights. If we increase the penalty weights further by, say, a factor of 10, then χ^2 increases

by ~25%. Thus, it is possible that the true shape of Nyx is more topographically rugged than the model, but the converse is not true. In other words, our model represents a lower bound on the irregularity of Nyx's shape.

Figure 6 shows plane-of-sky views of the models and Fig. 7 shows observed spectra, modeled spectra, and residuals. Table IV summarizes key parameters.

Nyx's 13-cm OC radar albedo (the OC radar cross section divided by the projected area) is 0.15 ± 0.075, an estimate that is near the middle of the distribution of reported NEA radar albedos, which have a mean and rms dispersion of 0.18 and 0.13. Nyx's absolute visual magnitude $H = 17.55$ (Pravec and co-workers, in preparation) is related to its visual geometric albedo p_v and effective diameter D_{eff} (that is, the diameter of a sphere with the same volume as the shape model) by (Bowell

TABLE IV
Physical Properties Derived from the Shape Model

Property	Value
Volume (km^3)	0.58 ± 0.2
D_{eff} (km)	1.04 ± 0.16
I_{short}/I_{long}	1.07 ± 0.11
I_{int}/I_{long}	1.05 ± 0.11
p_v ($H = 17.55$)	$0.16^{+0.08}_{-0.05}$
Radar albedo	0.15 ± 0.075
λ (°)	43 ± 30
β (°)	$+71 \pm 15$

Note. D_{eff} is the effective diameter. I_{short}, I_{long}, and I_{int} are the moments of inertia about the short, long, and intermediate principal axes. p_v is the optical geometric albedo and H is the absolute magnitude. λ and β are the ecliptic longitude and latitude of the spin vector.

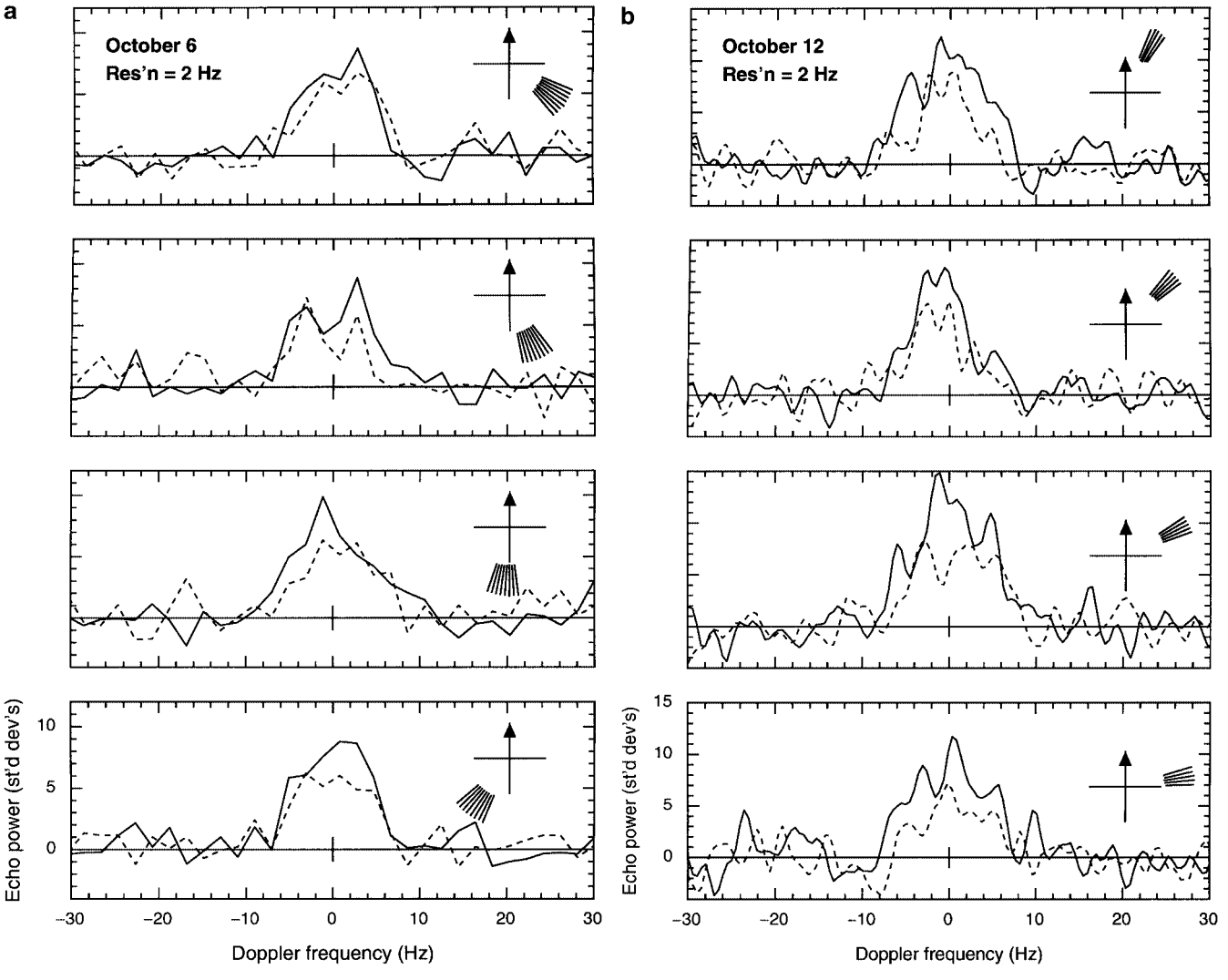

FIG. 4. Evolution of Goldstone echo power spectra on (a) October 6, (b) 12, and (c) 24 and 25. Rotation phase (time) increases from top to bottom and from left to right. The October 12 spectra are shown at 15° rotation phase intervals and the October 6, 24, and 25 spectra are shown at 30° rotation phase intervals.

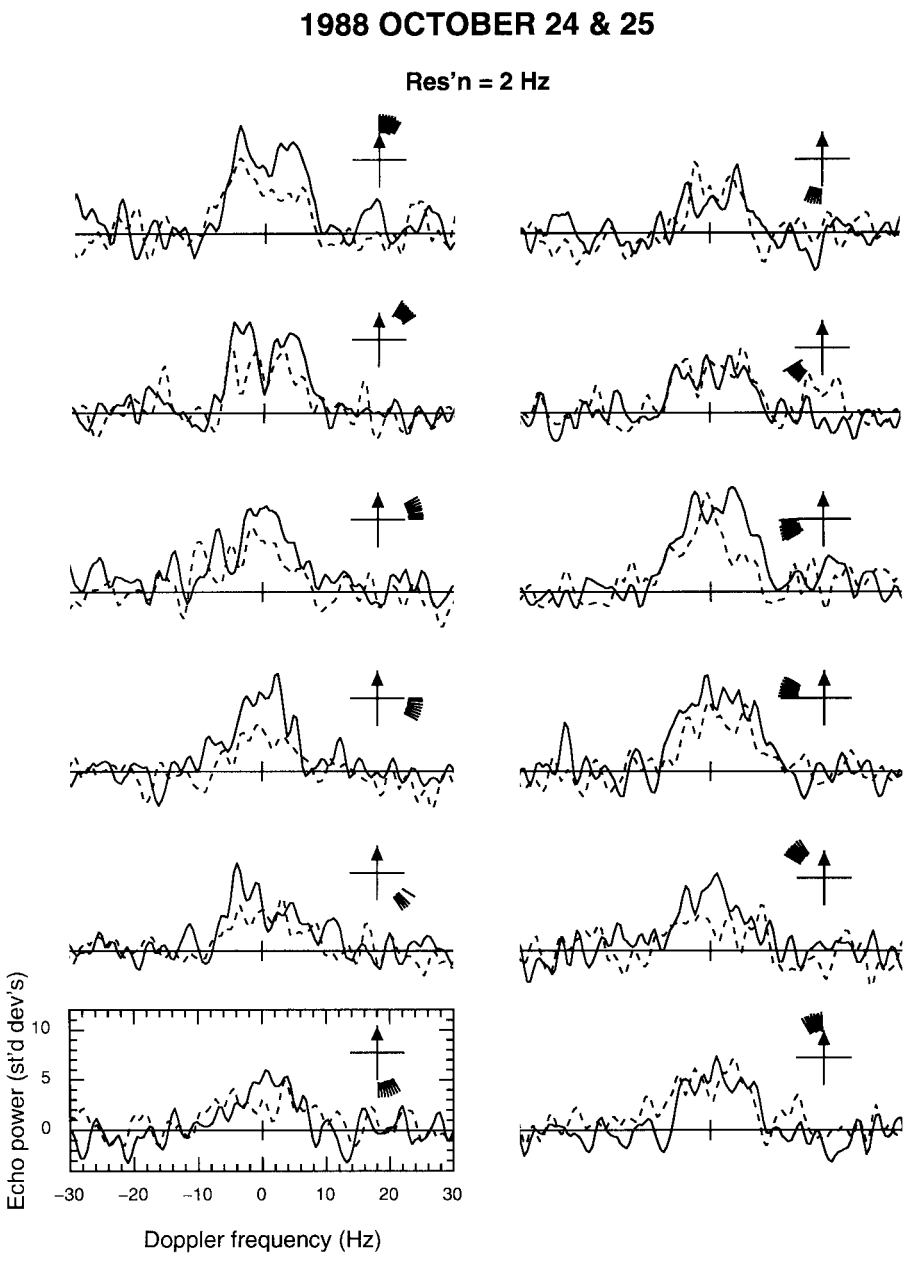

FIG. 4—*Continued*

et al. 1989): $\log(p_v) = 6.259 - 2\log(D_{\rm eff}) - 0.4H$. Our estimate of $D_{\rm eff}$ and its uncertainties yields $p_v = 0.16^{+0.08}_{-0.05}$, which is smaller than Vesta's albedo of 0.34 (Thomas *et al.* 1997) and the albedo of ∼0.3 estimated for the basaltic near-Earth asteroid 1996 JA1 (Spahr *et al.* 1997), but slightly larger than the albedo of 0.12 ± 0.03 estimated for 1459 Magnya (Tedesco 1989), the only other basaltic asteroid (Lazzaro *et al.* 2000) for which an albedo is available.

The visual albedo is consistent with Cruikshank *et al.*'s "rocky" thermal model, which assumes a sphere with the thermal inertia of bare rock, but it is in stark contrast with the results of the "standard" thermal model (Table I), which assumes a nonrotating sphere and the thermal inertia of a porous regolith. The visual albedo supports Cruikshank *et al.*'s interpretation that Nyx has a thermal inertia consistent with that of bare rock. If so, then Nyx, 6489 Golevka (Hudson *et al.* 2000), and perhaps 2100 Ra-Shalom (Shepard *et al.* 2000) may be the only radar-detected NEAs larger than ∼200 m in diameter known to have surfaces of mostly bare rock.

Burbine *et al.* (2001) examined visible-near infrared spectra of main-belt basaltic asteroids and their meteorite counterparts (the howardites, eucrites, and diogenites). They found that visual

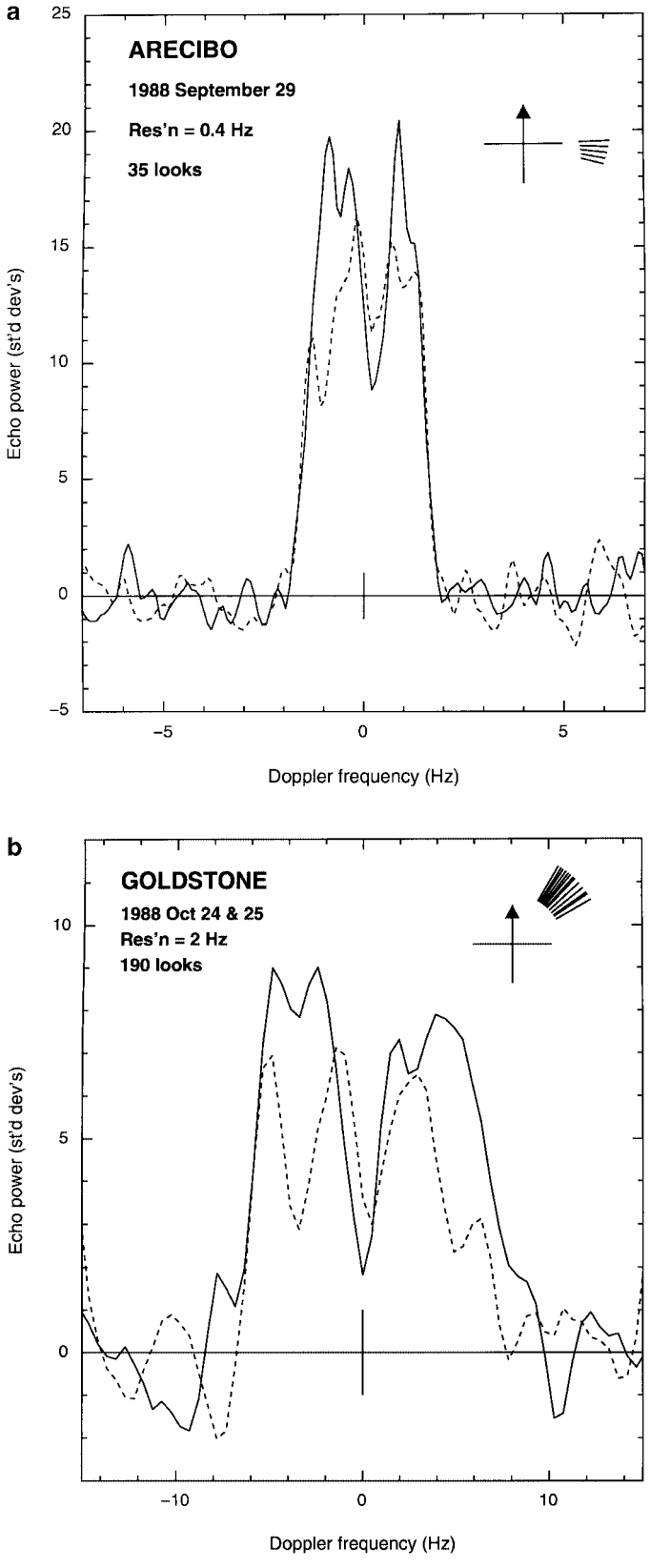

FIG. 5. (a) Arecibo and (b) Goldstone echo power spectra showing statistically significant central dips.

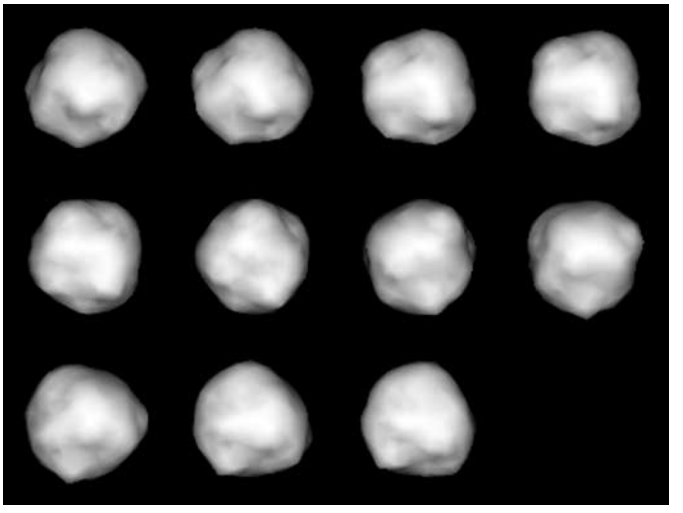

FIG. 6. Plane-of-sky renderings of the shape model. The model is shown at average rotation phases corresponding to its orientation in the spectra in Fig. 3. The renderings use Lambertian scattering and a phase angle of zero degrees.

albedo increases with decreasing particle grain size, suggesting that the relatively low visual albedo of Nyx is consistent with a surface that has coarse grains and is rugged at decimeter spatial scales (T. H. Burbine, personal communication).

For objects with low circular polarization ratios, the radar albedo can be related to the surface bulk density or porosity using an empirical expression derived from laboratory experiments (Garvin *et al.* 1985, Magri *et al.* 2001), an approach that could, in principle, constrain whether or not Nyx's surface is bare rock. However, the validity of the empirical relationship is difficult to ascertain due to Nyx's high circular polarization ratio, so we did not apply this approach to Nyx.

The shape model is somewhat irregular, is modestly asymmetric, and has pronounced topographic relief, including modest concavities. Fits to prominent dips in the spectra have $\sim 5\sigma$ residuals, hinting that the concavities could be even more pronounced or the topography more complicated. Nyx is very rough at decimeter spatial scales, which sets it apart from other NEAs for which shape models are available.

Nyx's irregular shape and its rough and apparently rocky surface may indicate that it is a geologically youthful impact product. Impact simulations between assemblages of spherical particles with uniform sizes and bulk densities (Leinhardt *et al.* 2000) have produced a suite of exotic shapes. More sophisticated simulations using particles with a distribution of sizes and shapes are desirable.

Nyx will approach within 0.14 AU of Earth in November 2004. Single-date SNRs at Arecibo could approach 200 and be adequate for delay-Doppler imaging and improved shape reconstruction at decameter spatial scales.

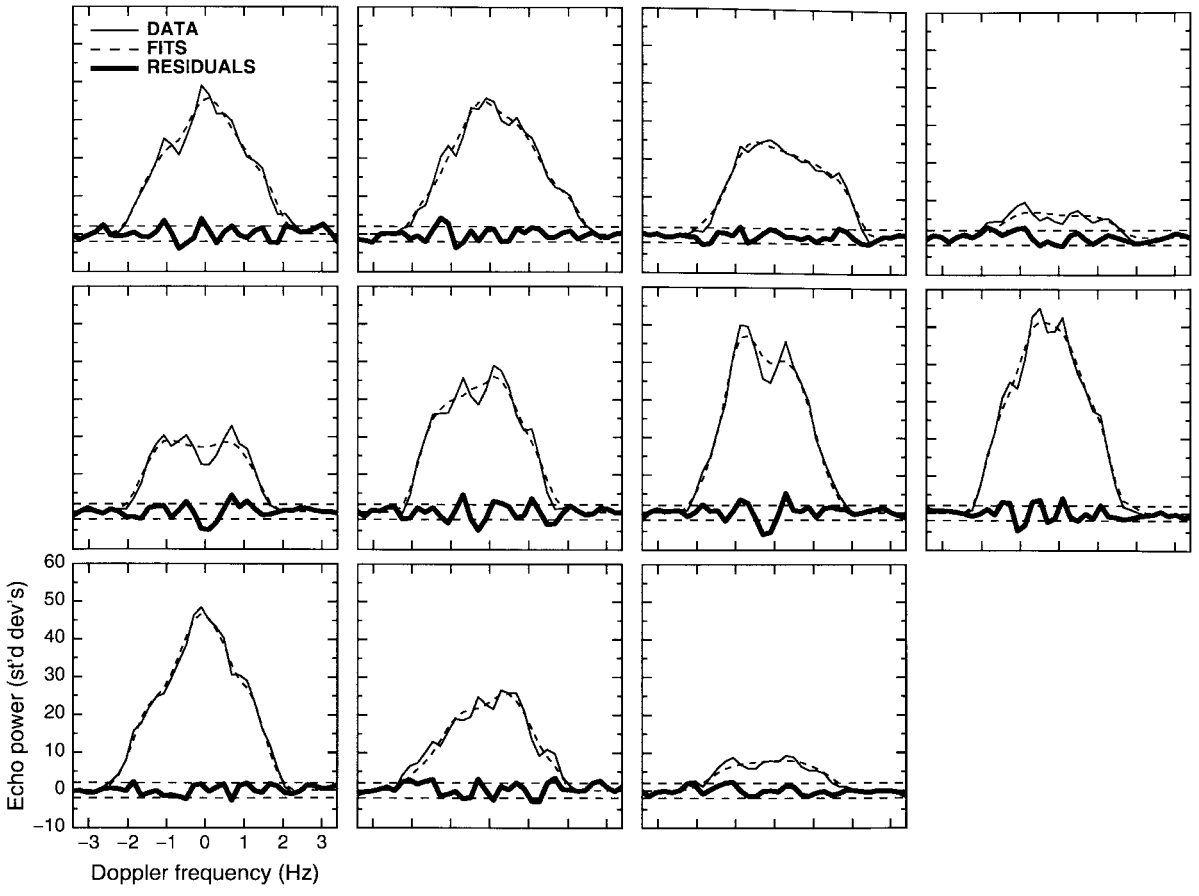

FIG. 7. Sequence of Arecibo CW spectra, modeled CW spectra, and residuals shown at ∼25° rotation phase intervals. Spectra are the same as those shown in Fig. 3. Dashed horizontal lines denote ±2 standard deviations.

ACKNOWLEDGMENTS

Part of this research was conducted at the Jet Propulsion Laboratory, California Institute of Technology, under contract with the National Aeronautics and Space Administration (NASA). Work at Washington State University was supported, in part, by a grant from NASA. Work at the Center for Astrophysics was supported, in part, by a grant from NASA. The Arecibo Observatory is part of the National Astronomy and Ionosphere Center, which is operated by Cornell University under a cooperative agreement with the National Sciences Foundation and with support from NASA.

REFERENCES

Benner, L. A. M., S. J. Ostro, J. D. Giorgini, R. F. Jurgens, D. L. Mitchell, R. Rose, K. D. Rosema, M. A. Slade, R. Winkler, D. K. Yeomans, D. B. Campbell, J. F. Chandler, and I. I. Shapiro 1997. Radar detection of near-Earth Asteroids 2062 Aten, 2101 Adonis, 3103 Eger, 4544 Xanthus, and 1992 QN. *Icarus* **130**, 296–312.

Benner, L. A. M., R. S. Hudson, S. J. Ostro, K. D. Rosema, J. D. Giorgini, D. K. Yeomans, R. F. Jurgens, D. L. Mitchell, R. Winkler, R. Rose, M. A. Slade, M. L. Thomas, and P. Pravec 1999. Radar observations of Asteroid 2063 Bacchus. *Icarus* **139**, 309–327.

Binzel, R. P., A. W. Harris, S. J. Bus, and T. H. Burbine 2001. Spectral properties of near-Earth objects: Palomar and IRTF results for 48 objects including spacecraft targets (9969) Braille and (10302) 1989 ML. *Icarus* **151**, 139–149.

Bowell, E., B. Hapke, D. Domingue, K. Lumme, J. Peltoniemi, and A. W. Harris 1989. Application of photometric models to asteroids. In *Asteroids II* (R. P. Binzel, T. Gehrels, and M. S. Matthews, Eds.), pp. 524–556. Univ. of Arizona Press, Tucson.

Burbine, T. H., P. C. Buchanan, R. P. Binzel, S. J. Bus, T. Hiroi, J. L. Hinrichs, A. Meibom, and T. J. McCoy 2001. Vesta, Vestoids, and the howardite, eucrite, diogenite group: Relationships and the origin of spectral differences. *Meteorit. Planet. Sci.* **36**, 761–781.

Cruikshank, D. P., D. J. Tholen, W. K. Hartmann, J. F. Bell, and R. H. Brown 1991. Three basaltic Earth-approaching asteroids and the source of the basaltic meteorites. *Icarus* **89**, 1–13.

Drummond, J. D., and W. Z. Wisniewski 1990. The rotational poles and shapes of 1580 Betulia and 3908 (1980 PA) from one apparition. *Icarus* **83**, 349–359.

Garvin, J. B., J. W. Head, G. H. Pettengill, and S. H. Zisk 1985. Venus global radar reflectivity and correlations with elevation. *J. Geophys. Res.* **90**, 6859–6871.

Howell, E. S., M. C. Nolan, L. DeRemer, and J.-L. Margot 2001. Arecibo radar observations of near-Earth Asteroid 2000 EE104. *Bull. Am. Astron. Soc.* **33**, 1153. [Abstract]

Hudson, S. 1993. Three-dimensional reconstruction of asteroids from radar observations. *Remote Sensing Rev.* **8**, 195–203.

Hudson, R. S., and S. J. Ostro 1994. Shape of Asteroid 4769 Castalia (1989 PB) from inversion of radar images. *Science* **263**, 940–943.

Hudson, R. S., and S. J. Ostro 1995. Shape and non-principal axis spin state of Asteroid 4179 Toutatis. *Science* **270**, 84–86.

Hudson, R. S., S. J. Ostro, R. F. Jurgens, K. D. Rosema, J. D. Giorgini, R. Winkler, R. Rose, D. Choate, R. A. Cormier, C. R. Franck, R. Frye, S. D. Howard, D. Kelley, R. Littlefair, M. A. Slade, L. A. M. Benner, M. L. Thomas, D. L. Mitchell, P. W. Chodas, D. K. Yeomans, D. J. Scheeres, P. Palmer, A. Zaitsev, Y. Koyama, A. Nakamura, and A. W. Harris 2000. Radar observations and physical modeling of Asteroid 6489 Golevka. *Icarus* **148**, 37–51.

Lazzaro, D., T. Michtchenko, J. M. Carvano, R. P. Binzel, S. J. Bus, T. H. Burbine, T. Mothe-Diniz, M. Florczak, C. A. Angeli, and A. W. Harris 2000. Discovery of a basaltic asteroid in the outer main belt. *Science* **288**, 2033–2035.

Leinhardt, Z. M., D. C. Richardson, and T. Quinn 2000. Direct *N*-body simulations of rubble pile collisions. *Icarus* **146**, 133–151.

Magri, C., G. J. Consolmagno, S. J. Ostro, L. A. M. Benner, and B. R. Beeney 2001. Radar constraints on asteroid regolith compositions using 433 Eros as ground truth. *Meteorit. Planet. Sci.* **36**, 1697–1709.

Mahapatra, P. R., S. J. Ostro, L. A. M. Benner, K. D. Rosema, R. F. Jurgens, R. Winkler, R. Rose, J. D. Giorgini, D. K. Yeomans, and M. A. Slade 1999. Recent radar observations of Asteroid 1566 Icarus. *Planet. Space Sci.* **47**, 987–995.

Marsden, B. G. 1980 PA. IAU Circ. *3499*.

Mitchell, D. L., S. J. Ostro, R. S. Hudson, K. D. Rosema, D. B. Campbell, R. Velez, J. F. Chandler, I. I. Shapiro, J. D. Giorgini, and D. K. Yeomans 1996. Radar observations of Asteroids 1 Ceres, 2 Pallas, and 4 Vesta. *Icarus* **124**, 113–133.

Mitchell, D. L., R. S. Hudson, S. J. Ostro, and K. D. Rosema 1998. Shape of 433 Eros from inversion of Goldstone radar Doppler spectra. *Icarus* **131**, 4–14.

Ostro, S. J., J. F. Chandler, A. A. Hine, I. I. Shapiro, K. D. Rosema, and D. K. Yeomans 1990. Radar images of Asteroid 1989 PB. *Science* **248**, 1523–1528.

Ostro, S. J., D. B. Campbell, J. F. Chandler, I. I. Shapiro, A. A. Hine, R. Velez, R. F. Jurgens, K. D. Rosema, R. Winkler, and D. K. Yeomans 1991. Asteroid radar astrometry. *Astron. J.* **102**, 1490–1502.

Ostro, S. J., D. B. Campbell, R. A. Simpson, R. S. Hudson, J. F. Chandler, K. D. Rosema, I. I. Shapiro, E. M. Standish, R. Winkler, D. K. Yeomans, R. Velez, and R. M. Goldstein 1992. Europa, Ganymede, and Callisto: New radar results from Arecibo and Goldstone. *J. Geophys. Res.* **97**, 18,227–18,244.

Ostro, S. J., R. F. Jurgens, K. D. Rosema, R. S. Hudson, J. D. Giorgini, R. Winkler, D. K. Yeomans, D. Choate, R. Rose, M. A. Slade, S. D. Howard, D. J. Scheeres, and D. L. Mitchell 1996. Radar observations of Asteroid 1620 Geographos. *Icarus* **121**, 46–66.

Ostro, S. J., P. Pravec, L. A. M. Benner, R. S. Hudson, L. Sarounova, M. D. Hicks, D. L. Rabinowitz, J. V. Scotti, D. J. Tholen, M. Wolf, R. F. Jurgens, M. L. Thomas, J. D. Giorgini, P. W. Chodas, D. K. Yeomans, R. Rose, R. Frye, K. D. Rosema, R. Winkler, and M. A. Slade 1999. Radar and optical observations of Asteroid 1998 KY26. *Science* **285**, 557–559.

Ostro, S. J., R. S. Hudson, L. A. M. Benner, M. C. Nolan, J.-L. Margot, J. D. Giorgini, R. F. Jurgens, R. Rose, and D. K. Yeomans 2000. Radar observations of Asteroid 4486 Mithra. *Bull. Am. Astron. Soc.* **32**, 1003. [Abstract]

Shepard, M. K., L. A. M. Benner, S. J. Ostro, A. W. Harris, K. D. Rosema, I. I. Shapiro, J. F. Chandler, and D. B. Campbell 2000. Radar observations of Asteroid 2100 Ra-Shalom. *Icarus* **147**, 520–529.

Spahr, T. B., C. W. Hergenrother, S. M. Larson, M. Hicks, B. G. Marsden, G. V. Williams, D. J. Tholen, R. J. Whiteley, and D. J. Osip 1997. The discovery and physical characteristics of 1996 JA1. *Icarus* **129**, 415–420.

Tedesco, E. F. 1989. Asteroid magnitudes, UBV colors, and IRAS albedos and diameters. In *Asteroids II* (R. P. Binzel and M. S. Matthews, Eds.), pp. 1090–1138. Univ. of Arizona Press, Tucson.

Thomas, P. C., R. P. Binzel, M. J. Gaffey, A. D. Storrs, E. N. Wells, and B. H. Zellner 1997. Impact excavation on Asteroid 4 Vesta: Hubble Space Telescope results. *Science* **277**, 1492–1495.

Veverka, J., P. C. Thomas, J. F. Bell III, M. Bell, B. Carcich, B. Clark, A. Harch, J. Joseph, P. Martin, M. Robinson, S. Murchie, N. Izenberg, E. Hawkins, J. Warren, R. Farquhar, A. Cheng, D. Dunham, C. Chapman, W. J. Merline, L. McFadden, D. Wellnitz, M. Malin, W. M. Owen, Jr., J. K. Miller, B. G. Williams, and D. K. Yeomans 1999. Imaging of Asteroid 433 Eros during NEAR's flyby reconnaissance. *Science* **285**, 562–564.